CANADIAN JOURNAL OF REMOTE SENSING
2020, VOL. 46, NO. 6, 784–802
https://doi.org/10.1080/07038992.2021.1872374



# Object-Based Wetland Classification Using Multi-Feature Combination of Ultra-High Spatial Resolution Multispectral Images

# Classification orientée-objet des milieux humides à l'aide d'une combinaison multi-paramètres d'images multispectrales à résolution spatiale ultra-haute

Renfang Geng[a], Shuanggen Jin[a,b], Bolin Fu[c], and Bin Wang[d]

[a]School of Remote Sensing and Geomatics Engineering, Nanjing University of Information Science and Technology, Nanjing 210044, China; [b]Shanghai Astronomical Observatory, Chinese Academy of Sciences, Shanghai 200030, China; [c]College of Geomatics and Geoinformation, Guilin University of Technology, Guilin 541004, China; [d]School of Geography and Information Engineering, China University of Geosciences, Wuhan 430074, China

**ABSTRACT**

The Unmanned Aerial Vehicle (UAV) and Google Earth (GE) RGB images have ultra-high spatial resolution. But it is difficult to get a high classification accuracy due to the poor spectral resolution. In this article, the object-based wetland classification is investigated using multi-feature combination of ultra-high spatial resolution multispectral images (MSI). A Gram-Schmidt (GS) transformation is used to fuze Sentinel-2A data with UAV and GE RGB images, respectively, in order to obtain the ultra-high spatial resolution MSI as data sources. Three different feature combination classification scenarios are constructed for fusion GE and UAV MSI, respectively, based on selected features. The object-based random forest (RF) algorithms with parameters (*mtry* and *ntree*) optimization are used to carry out finer wetland classification. Results show that the fusion GE and UAV MSI have good applicability in the finer wetland classification, especially the fusion UAV images, and integrating multi-source features could improve classification accuracy. Both data sources reach the highest accuracy in scenario3. The overall accuracy of fusion UAV image scenario3 is 94.31% (Kappa = 0.9353), and that of fusion GE image scenario3 is 87.37% (Kappa = 0.8528). The contribution of different features to wetland classification is obtained with spectral and vegetation indexes, texture, geometric and contextual features.

**RÉSUMÉ**

Les images RGB de drones (UAV) et de Google Earth (GE) ont une résolution spatiale ultra-haute. Cependant, il est difficile d'obtenir une grande précision de classification en raison de la faible résolution spectrale. Dans cet article, une classification des milieux humides orientée objet est étudiée à l'aide d'une combinaison multi-paramètres d'images multispectrales à résolution spatiale ultra-haute (MSI). Une transformation Gram-Schmidt (GS) est utilisée pour fusionner les données Sentinel-2A avec des images UAV et GE RGB, respectivement, afin d'obtenir un MSI à résolution spatiale ultra-haute comme sources de données. Trois scénarios différents de classification des combinaisons de paramètres sont construits pour la fusion GE et UAV MSI, respectivement, en fonction des paramètres sélectionnés. Les algorithmes de forêt aléatoire (RF) orientés-objets avec optimisation des paramètres (*mtry* et *ntree*) sont utilisés pour effectuer une classification plus fine des milieux humides. Les résultats montrent que les fusions GE et UAV MSI ont une bonne applicabilité dans la classification plus fine des zones humides, en particulier la fusion des images de drones, et l'intégration de paramètres multi-sources pourraient améliorer la précision de la classification. Les deux sources de données atteignent la plus grande précision pour le scénario 3. La précision globale du scénario 3 pour la fusion d'une image de drone est de 94,31% (Kappa = 0,9353), et celle du scénario 3 pour la fusion d'une image GE est de 87,37% (Kappa = 0,8528). La contribution de différentes caractéristiques à la classification des milieux humides est obtenue à l'aide d'indices spectraux et de végétation et des paramètres de texture, de géométrie et contextuels.

**ARTICLE HISTORY**
Received 25 September 2020
Accepted 3 January 2021

**CONTACT** Shuanggen Jin sgjin@shao.ac.cn; Bolin Fu fubolin@glut.edu.cn

## Introduction

Wetlands are some of the most important and valuable ecosystems that provide many well-documented ecosystem goods and services, such as flood control and drought prevention, water purification and groundwater recharge, sediment retention and stabilization, runoff control and climate regulation, etc. (Mahdavi et al. 2017; Mahdianpari et al. 2020; Powers et al. 2012; Ji et al. 2015). Over the past century, wetlands are increasingly disturbed by human activities, and a large number of wetlands have been forcibly converted into agricultural and urban land with a global trend of disappearance or degradation (Davidson 2014; Alvarez-Cobelas et al. 2007). Wetland degradation will not only lead to its decline of ecosystem services but also affect the health and well-being of all human beings. Therefore, it is urgent for us to properly manage and protect wetlands.

Nowadays, satellite remote sensing technology is fast and efficient for monitoring the wetland ecosystem when compared to conventional field work, and has been widely used in wetland classification, dynamic change monitoring and resource investigation, etc. (Chen et al. 2020; Lv et al. 2019; Cao et al. 2018). Currently, the MSI with medium and high spatial resolution is the main data source for wetland classification, such as Sentinel-2A/B, Worldview-2 and GF-1, etc. For example, Lou et al. (2020) used the GF-1 and ZY-3 data to conduct the Honghe National Nature Reserve marsh vegetation mapping, and the results showed that the performance of GF-1 image applied to marsh vegetation mapping is higher than that of ZY-3 image, but both images had higher classification accuracy for forest, cropland, shrubs, and open water. Wang et al. (2019) selected Worldview-2 and Landsat-8 images to carry out the Linhong Estuary wetland Land-Cover Classification in Lianyungang, and pointed out that the high-resolution Worldview-2 MSI was more suitable for small-scale wetland land use classification than the medium-resolution Landsat-8 images. Unfortunately, these high spatial resolution images, such as Worldview-2, Ikonos, Quickbird or even Pleiades, have an associated high cost of data acquisition and cannot allow sufficiently frequent sampling to monitor wetland habitats continuously (Alvarez-Vanhard et al. 2020).

In recent years, GE tool (http://www.google.com/earth/index.html), released in 2005, as a free and open data platform, has developed rapidly and widely used in many fields, such as data collection, validation, visualization, and data integration, etc. (Mering et al. 2010; Kaimaris et al. 2011; Yu and Gong 2012; Clark et al. 2010; Pulighe et al. 2016). The GE image is an integration of very high spatial resolution images and is free, while its resolutions can achieve up to submeter levels (Guo et al. 2016). And the high spatial resolution GE images have only three bands: red, green, and blue (RGB). Due to the poor spectral information, there have not been too many finer wetlands mapping based on GE images, as they are mainly used for urban land use classification, urban impervious surface area extraction and village buildings identification (Hu et al. 2013; Huang et al. 2018; Guo et al. 2016). For instance, Guo et al. (2016) selected GE RGB images to perform village building identification at Savannakhet province in Laos with pixel-based supervised machine learning methods, and the experimental results showed that the AdaBoost method achieves an overall accuracy of 96.22% while the CNN method is an overall accuracy of 96.30%. Hu et al. (2013) selected a GE image for a case study in Wuhan City to perform an object-based land use classification. It was found that high spatial resolution GE image had some potential for regional land use mapping with a 78.07% overall accuracy. And the main factor that restricts the improvement of classification accuracy is its poor spectral characteristics, with only three bands of red, green and blue, and the gray value of each band is only between 0 and 255.

Low-altitude UAVs have developed rapidly in recent years, provided a new low-cost remote sensing data source with unrivaled properties, which can acquire multi-angle and very high-resolution remote sensing data based on the user's interests, and less restricted by the condition of landing sites or cloud cover (Anderson and Gaston 2013; Alvarez-Vanhard et al. 2020). Due to this flexibility and efficiency, they are very popular in wetland mapping and monitoring, a good supplement to satellite data. (Bendig et al. 2015; Li and Li 2014; Watts et al. 2012). Because of the complex types of wetland vegetation, current wetland classification using UAV remotely sensed data is dominated by multispectral or hyperspectral images. For instance, Cao et al. (2018) used UAV hyperspectral images and digital surface model (DSM) to carry out offshore mangrove wetlands classification using OBIA method. Abeysinghe et al. (2019) selected the UAV MSI and machine learning classifiers to mapping wetland invasive *Phragmites australis*. Only a few studies used the consumer-level UAV with ordinary optical cameras to carry out wetland vegetation classification. Pande-Chhetri et al. (2017) used high-resolution UAV RGB images and OBIA method to mapping the Eagle Bay wetland in South Florida,

considering the multi-source features. But the classification accuracy was relatively low, the scenario of highest overall accuracy was only 70.78%. Wetlands need a continuous observation and monitoring, which might become a complex task. And only the RGB sensor should be considered as a low-cost application (Brook et al. 2020).

Both GE and UAV RGB images have high spatial resolution with poor spectral characteristics, but the spectral information is the most important in wetland vegetation classification. Therefore, they have obvious limitations in finer and high accuracy wetland land use mapping. To solve this problem, some scholars have fused UAV RGB image with Sentinel-2A/B and Landsat-8 data to make up for the limitations of UAV RGB image spectral resolution. For example, Jenerowicz and Woroszkiewicz (2016) presented fusion of Landsat-8 and UAV image for distinguishing agricultural crop types. Zhao et al. (2019) fused UAV and Sentinel-2A images to map finer crop distribution using pixel-based machine learning classification method. Alvarez-Vanhard et al. (2020) firstly tested spectral synergies between UAV and Sentinel-2 data to map habitat mapping, which illustrated well the great potential of combined UAV and satellite data.

Wetland vegetation type is complex and spectral confusion is more serious with many small or patchy habitat types. Therefore, it is more difficult than cropland/urban land use classification. Currently, there is no relevant research on small-scale wetland finer classification using ultra-high spatial resolution GE images to explore its applicability in wetland mapping. Although the UAV RGB images have been used for wetlands mapping, the classification accuracy is still low due to its poor spectral resolution. And there are also some attempts to combine the pro and cons of space-borne and UAV RGB data to perform crop classification based on the pixel-based method while lacking detailed exploration in complex wetland classification. Moreover, the pixel-based method cannot make use of the spatial information of ultra-high spatial resolution GE and UAV images, and the "salt and pepper" noise is serious (Duro et al. 2012; Blaschke 2010; Ma et al. 2017).

In view of this, the purpose of this study is to test the applicability for the fusion of GE or UAV RGB images with Sentinel-2A data in finer karst wetland vegetation classification. In order to overcome the effect of "salt and pepper" noise and make full use of the information of high spatial resolution images, object-based image analysis (OBIA) is used. The parameters, named *ntree* and *mtry* are optimized in object-based RF algorithm model, in order to improve classification accuracy. A further objective has been to evaluate the contribution of multidimensional features to wetland classification through the multi-feature combination scenarios and RF variable importance. This study can provide a new idea for data source selection, segmentation parameters selection, object-based RF parameters optimization and classification features selection. Section 2 shows the data and methods, results and analysis are presented in Section 3, and discussion and conclusions are given in Sections 4 and 5, respectively.

## Data and methods

### Study area

The Huixian wetland is a comprehensive natural wetland composed of swamps, rivers, and lakes, and has significant characteristics of a karst area, located in Guilin, Guangxi province, China (25°01′30″N∼25°11′15″N, 110°08′15″E∼110°18’00″E) (Figure 1). It is part of the Lijiang River system and plays a key role as water supply resources for Guilin city, known as the "kidney of Lijiang" (Xiao et al. 2019). In 2012, it was listed as a National Wetland Park pilot by the State Forestry Administration and named as "Huixian Karst National Wetland Park in Guilin, Guangxi province, China." Since the 1970s, the ecological system of Huixian karst wetland has been seriously affected due to the intensification of human interference and lack of effective protection measures. Nowadays, the water surface has gradually shrunk, the wetland area is decreasing and the core area is less than 6 $km^2$ in the dry season. The diversity of plants and animals has decreased, part of the wetland center is occupied by fish ponds and farmland. In addition, invasive species such as *Hyacinth* and *Amazonian snail* are threatening the few remaining wild plant species (Mingwu et al. 2010).

### Data

The original UAV remotely sensed images were captured by FC220 camera mounted on the DJI Royal Mavic Pro UAV, with lens Angle of −90°, course overlap rate of 80% and side overlap rate of 65%. The data acquisition time was 10:30 am on August 26, 2018, when the weather was clear and cloudless, four flight were carried out flying at an altitude of 105 m. A Pix 4 D Mapping software was selected do the UAV image processing to obtain digital orthophoto model (DOM) required to construct remotely sensed

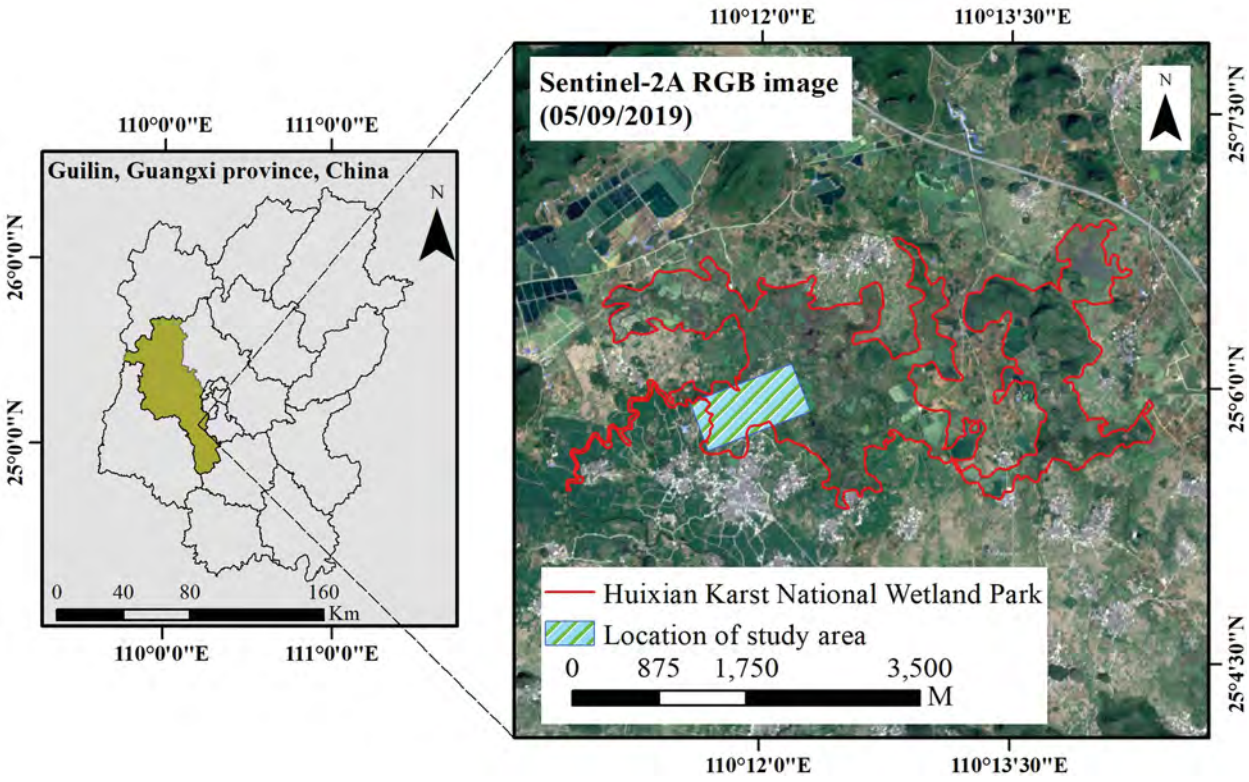


**Figure 1.** Study area situated in Guilin (Guangxi province, China).

**Table 1.** Summary of remotely sensed datasets used for this study.

| Sensor name | Sensor time | Band information | Resolution (m) |
|---|---|---|---|
| Sentienl-2A | 21/08/2018 | Red + Green + Blue + NIR | 10 |
| Sentienl-2A | 05/09/2019 | Red + Green + Blue + NIR | 10 |
| UAV Data | 26/08/2018 | Red + Green + Blue | 0.10 |
| GE Data | 04/09/2019 | Red + Green + Blue | 0.27 |

recognition model. In addition, some UAV images preprocessing operations, such as geometric correction, image mosaic, homogenizing, and clipping (1,100 m × 510 m), were carried out. Finally, the spatial resolution of UAV images was all down-sampled to 0.1 m on considering both the efficiency of image classification and the classification refinement level. The GE image with the 0.27 m spatial resolution was downloaded via free software called 91 weitu (http://www.91weitu.com/), whose GE images is from GE 7.1.8.3036 (32-bit), and the sensor time on September 4, 2019. Similarly, the GE image was geometrically corrected.

The Sentinel-2A images were acquired from the European Space Agency Sentinel Data Hub (https://scihub.copernicus.eu/) for the August 21, 2018 and September 5, 2019 with the MSI instrument. They were closest to the acquisition time of GE and UAV images. And the Sentinel Application Platform (SNAP) was used to preprocess the Sentinel-2A data. A summary of the image datasets used in this study can be found in Table 1.

Apart from acquiring the high spatial resolution UAV RGB images of the study site, field surveys for the characteristics and spatial distribution of wetland vegetation clusters were carried out synchronously. A sub-meter handheld GPS device was used to record the precise locations of samples. From the filed experience, it was found that vegetation types of the study area were complex, dominated mixed forest and mixed herbaceous vegetation (Table 2). In addition, the invasive hyacinth also occupied a large proportion, mainly distributed in karst lakes and mixed with lotus. And the sampling data were divided randomly in half for training and testing, respectively (Table 2).

## Methodology

In this study, the GE and UAV RGB images fused with Sentinel-2A data, respectively, to achieve high precision and detailed small-scale wetland classification using object-based RF algorithm. The classification scheme mainly consisted of four steps (Figure 2): (1) fusion of GE and UAV images with Sentinel-2A, respectively, to obtain GE and UAV MSI as classification remote sensing datasets; (2) the Fractal Net Evolution Approach (FNEA) Multi-Resolution

**Table 2.** Classes and samples used in the classification.

| Classification type | Vegetation association | GE training samples | GE testing samples | UAV training samples | UAV testing samples |
|---|---|---|---|---|---|
| Paddy | None | 39 | 39 | 44 | 44 |
| Exposed land | Uncultivated farmland, River floodplains | 49 | 48 | 46 | 45 |
| Mixed forest | Linden, Bamboo, Paliurus | 71 | 70 | 83 | 83 |
| Mixed grass | Bermuda grass, Eleusine indica, Paspalum | 68 | 67 | 67 | 66 |
| Hyacinth | None | 31 | 31 | 41 | 41 |
| Lotus | None | 32 | 32 | 37 | 37 |
| Road-building | Road, Wooden trestle, Building | 30 | 30 | 38 | 37 |
| Water | Karst river, Karst lake | 56 | 55 | 52 | 52 |
| Shadow | None | – | – | 53 | 52 |

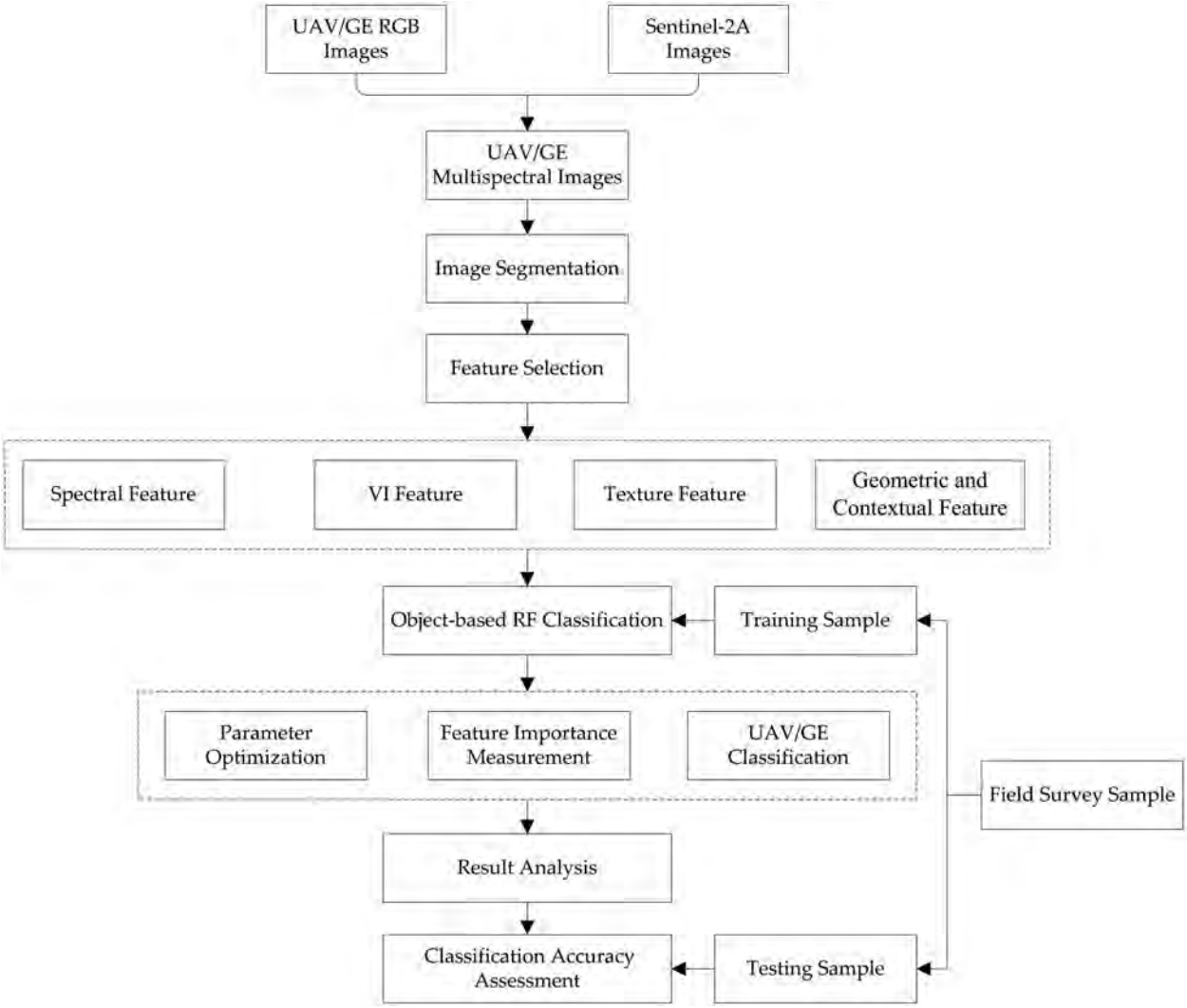


**Figure 2.** Flowchart of object-based wetland vegetation identification.

Segmentation (MRS) was used to segment the images with a selection of the optimal segmentation parameters (*scale*, *shape* and *compactness*); (3) feature extraction from fusion GE and fusion UAV MSI images, respectively, including spectral features, vegetation indexes, texture features, geometric and contextual features, and multi-feature combination classification scenarios were built; (4) object-based RF algorithm models were conducted, and the parameters, named *ntree* and *mtry* were optimized; (5) classification accuracy assessment was applied with overall accuracy (OA), kappa coefficient (Kappa), user's accuracy (UA), produce's accuracy (PA). The contribution of multi-features used in this study for wetland finer classification was analyzed.

### *Image fusion*

Image fusion is to process the multi-source data with redundant or complementary information based on certain rules or algorithms, in order to obtain more

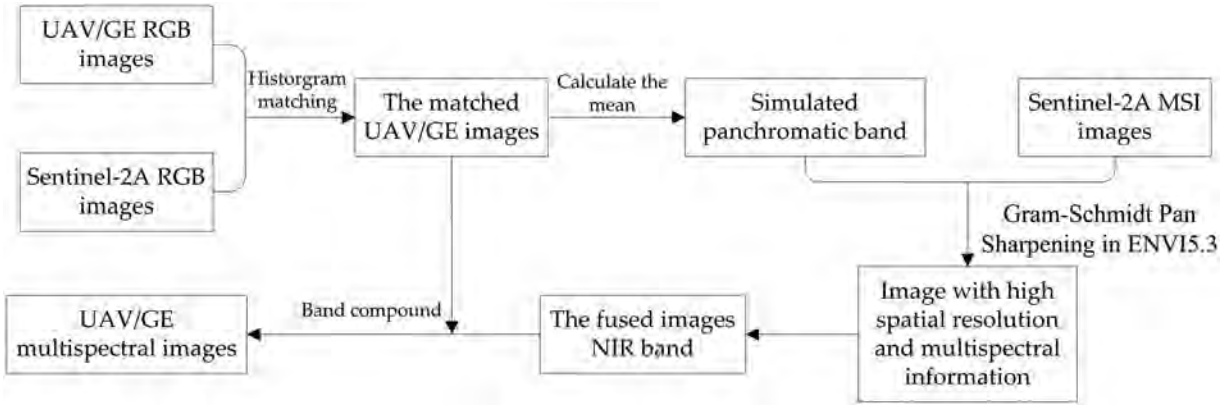


**Figure 3.** The flowchart of UAV/GE and Sentinel-2A images fusion using GS transformation.

accurate and richer information than any single data, and generate a composite image with new spatial and spectral characteristics. In this study, a GS pansharpening algorithm was used to fuze GE image and UAV image with Sentinel-2A data, respectively. This fusion algorithm could better improve the spatial details and spatial resolution of the original image while maintaining the spectral physical properties to the maximum extent (Mhangara et al. 2020; Tao et al. 2015). Before image fusion, a histogram matching was conducted for GE and UAV RGB image using the Sentinel-2A RGB images of the corresponding date, respectively. Then, calculated the mean of matched GE image and UAV image and regarded them as the high spatial resolution bands while the Sentinel-2A was the low-resolution MSI in GS image fusion. Finally, the NIR bands generated by fusion and matched GE and UAV image were taken out for composite band to obtain the fusion GE and UAV MSI. A detailed process is shown in Figure 3. The NIR band from fuzing GE/UAV and Sentinel-2A, the normalized difference vegetation index (NDVI) and normalized difference water index (NDWI) calculated the fuzing GE/UAV image are shown in Figure 4.

### *Image segmentation*

Image segmentation is a critical and important step in object-based classification, which is the process of dividing the image into spatially cohesive regions. The FNEA MRS probably the most popular algorithm in wetland vegetation identification, which segments the imagery into spectrally homogeneous, contiguous image objects in a bottom-up region-merging approach (Hossain and Chen 2019; Belgiu and Drăguţ 2014). Segmentation results are greatly influenced by the image quality, the number of image bands, the image resolution and the complexity of the scene (Belgiu and Drăguţ 2014). It is very important to select reasonable FNEA MRS parameters, both "under segmentation" and "over segmentation" will influence the final classification results (Belgiu and Drăguţ 2014; Drăguţ et al. 2014). In the FNEA MRS approach, there are three important parameters: *scale*, *shape* and *compactness*. And among them, the *scale* index is considered to be the most important parameter, a hot topic in FNEA MRS, which can make a greater impact on classification accuracy compared with the other two parameters. For example, Drăguţ et al. (2010) developed a scale parameter automatic selection tool for the eCognition software in 2010, named estimation of scale parameter (ESP), and this tool was improved in 2014 (Drăguţ et al. 2014), general said the improved tools for the ESP2, which could work on multiple layers compared with ESP. For the other two parameters, the optimization is mostly based on experience and trail-and-error fashion. For instance, Whyte et al. (2018) used trail-and-error fashion to optimize the FNEA MRS parameters when mapping the Greater St. Lucia Wetland Park using object-based machine learning algorithms. And the results showed that a low *shape* ratio produced the best segmentation results.

In this present study, the bands involved in the FNEA MRS included red, green and blue, intensity from HSI color space, red green ratio index (RGRI), based on fuzing GE/UAV images. And the weightings were set to 1,1,1,2,2, respectively. The MRS parameters weightings of *shape* and *compactness* were chosen through trial and error. Based on the vision analysis, *shape* and *compactness* was set as 0.3 and 0.5 respectively.

The ESP2 tool was used to choose the optimal scale parameter. This method relies on the potential of the local variance (LV) to detect scale transitions in geospatial data and identifies patterns in data at three different scales, ranging from fine objects (Level 1) to

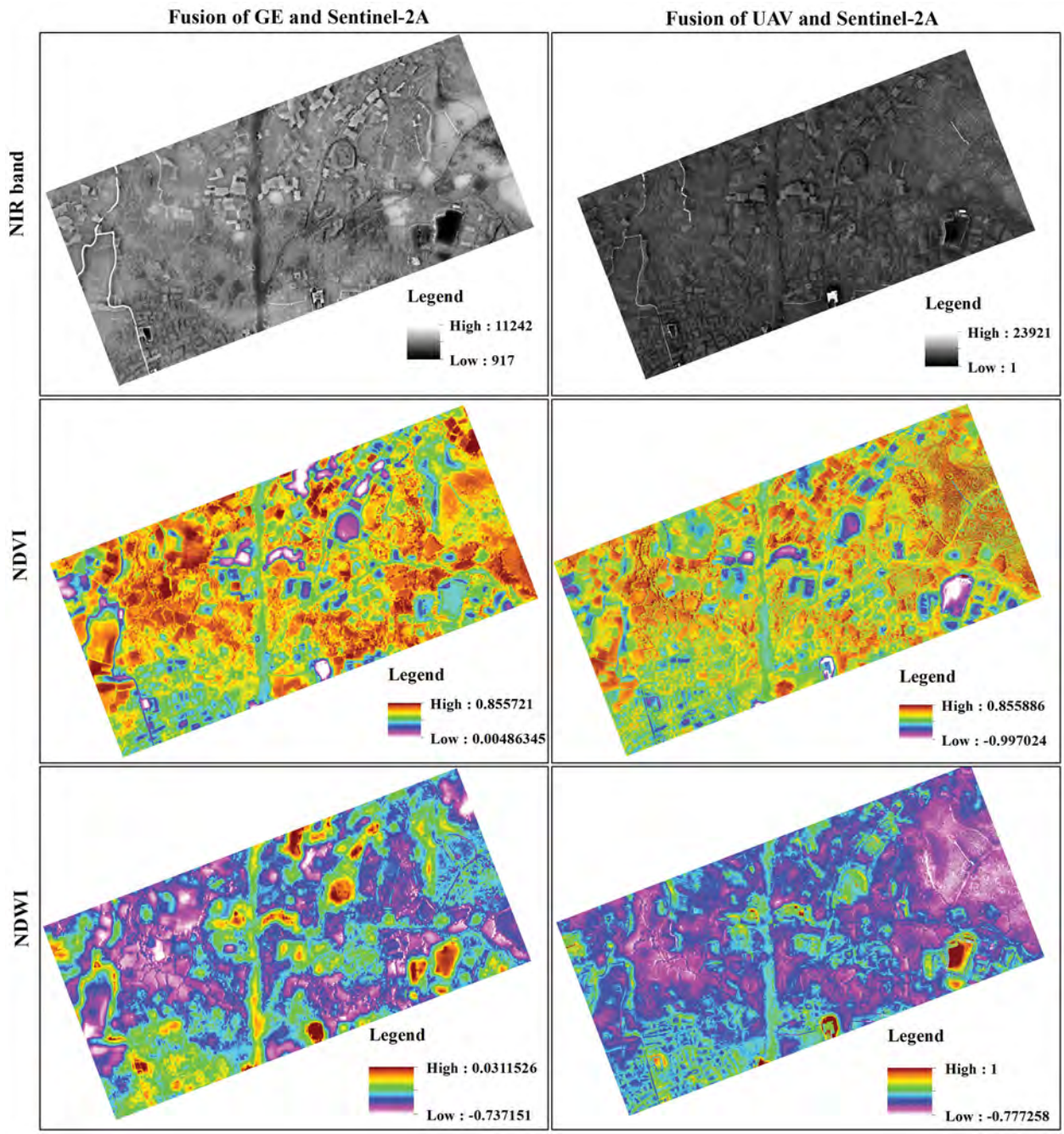


**Figure 4.** Image fusion results of NIR band and calculated vegetation index.

broader regions (Level 3). And the different *scale* parameters correspond to the inflection points of the LV curve, selecting the appropriate *scale* index can use the appropriate segmented objects to represent ground features in detail and precisely. After comparative analysis for the inflection points of the LV curve, fine scale factor of the fuzing GE and UAV images was set as 72 and 238, respectively. Finally, 4,260 and 9,282 segmentation objects were obtained, respectively. The local MRS results of fusion GE and UAV MSI are shown in Figure 5.

### *Feature extraction*

Following the image segmentation step, feature extraction represents another fundamental step in object-based classification. The ideal variables should make the segmented image objects highly separable (Duro et al. 2012). Due to the complexity of wetland vegetation types, multi-source object features were considered including spectral features, vegetation indexes, texture features, geometric features and contextual variables, based on fuzing GE and UAV images, as listed in Table 3. (1) Spectral bands, including mean

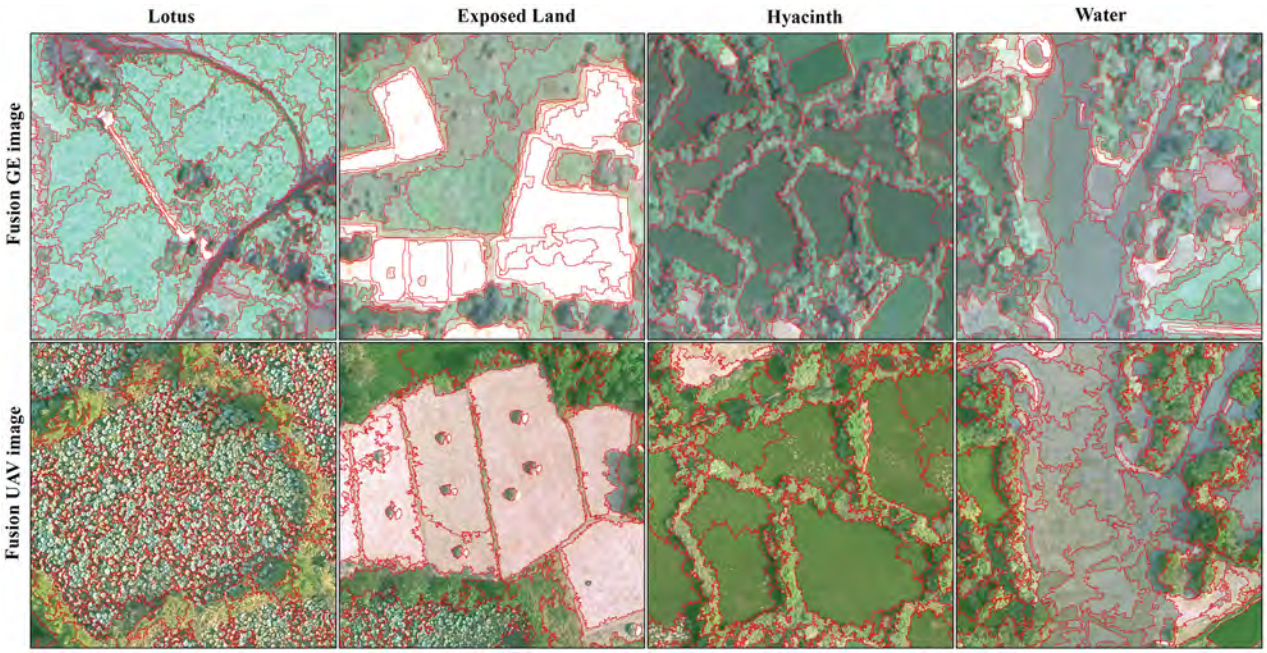


**Figure 5.** Local MRS results of fuzing GE and UAV images.

**Table 3.** Object features used for classification.

| Object features | Description |
|---|---|
| Spectral features | 18 Spectral features, including mean and standard deviation of R, G, B, NIR, H, S, I, and PCA. Brightness, and max.diff. |
| Vegetation indices | 15 VIs, including RGRI, NGBDI, NGRDI, EXG, VDVI, NDVI, NDWI, RVI, GNDVI, DVI, EVI2, TVI, SAVI, TTVI, and MSAVI2 |
| Textural features | 24 Textural features, including ASM, CON, COR, ENT, HOM, MEAN, DIS, and StdDev calculated using GLCM with three bands (band PCA, band I, and band NIR). |
| Shape and contextual features | 19 Geometric and Contextual Features, including Border Index, Area, Compactness, Y Max, Shape Index, Y Distance to Scene Bottom Border, X Center, Volume, Length/Width, X Distance to Scene Left Border, Length, Rectangular Fit, Y Center, Number of Pixels, X Max, Average Length of Edges (Polygon), Asymmetry, Width, and Border Length |

**Table 4.** Vegetation indices involved and their calculation formulas.

| Indices (VIs) | Formula | Description |
|---|---|---|
| RGRI | Red/Green | Red green ratio index |
| NGBDI | (Green-Blue)/(Green + Blue) | Normalized green-blue difference index |
| NGRDI | (Green-Red)/(Green + Red) | Normalized green-red difference index |
| EXG | 2*Green-Red-Blue | Excess green |
| VDVI | (2*Green-Red-Blue)/(2*Green + Red + Blue) | Visible-band difference vegetation index |
| NDVI | (NIR-Red)/(NIR + Red) | Normalized difference vegetation index |
| NDWI | (Green-NIR)/(Green + NIR) | Normalized difference water index |
| RVI | NIR/R | Ratio vegetation index |
| GNDVI | (NIR-Green)/(NIR + Green) | Green normalized difference vegetation index |
| DVI | NIR-Red | Difference vegetation index |
| EVI2 | 2.5*((NIR-Red)/(NIR + 2.4*Red)+1) | Two-band enhanced vegetation index |
| TVI | sqrt((NIR-Red)/(NIR + Red)+0.5) | Transformed vegetation index |
| SAVI | (1 + 0.5)*(NIR-Red)/(NIR + Red + 0.5) | Soil adjusted vegetation index |
| TTVI | sqrt(abs((NIR-Red)/(NIR + Red)+0.5)) | Thiam's transformed vegetation index |
| MSAVI2 | (2*(NIR + 1)-sqrt((2*NIR + 1)○2-8*(NIR-Red)))/2 | Adjusted vegetation index 2 |

and standard deviation of red, green, blue, near infrared (NIR) and first component of principal component analysis (PCA) for RGB bands, hue (H), saturation (S) and intensity (I) from HSI color space. In addition, brightness and max.diff (maximum intensity difference) were considered. (2) 15 vegetation indices (Table 4) were chosen, including red green ratio index (RGRI), normalized difference vegetation index (NDVI) and normalized difference water index (NDWI), etc. (3) texture features based on Gray level co-occurrence matrix (GLCM) (Table 3), including mean, variance, entropy and angular second moment,

Table 5. The information of experimental programs.

| GE scenario | UAV scenario | Description |
|---|---|---|
| 1 | 1 | Spectral + VI Features |
| 2 | 2 | Spectral + VI + GLCM Texture (PCA, I, and NIR) Features |
| 3 | 3 | Spectral + VI + GLCM Texture (PCA, I, and NIR) + Shape and Contextual Features |

etc (Lu et al. 2014; Szantoi et al. 2015). Among them, due to the high similarity between each band, only texture features of PCA, I and NIR were extracted in order to reduce data redundancy. (4) Compared with pixel-based classification, OBIA can consider the adjacency relation of each segmented object to extract the geometric and contextual features of the objects (Canisius et al. 2011; Moffett and Gorelick 2013). 19 geometric and contextual features that has been frequently used in previous studies were chosen, such as border index, shape index and asymmetry, etc., as listed in Table 3.

### Object-based RF algorithm

RF is an ensemble classifier algorithm, proposed by Breiman Leo and Adele Cutler in 2001 (Breiman 1996; Breiman 2001). Compared with other machine learning classifiers, RF works well with the curse of dimensions and highly correlated data, less sensitive to the quality of training samples and to overfitting (Belgiu and Drăguţ 2016). And it is very popular in wetland information extraction from hyperspectral, multispectral, radar, LiDAR and thermal remote sensing imagery (de Almeida Furtado et al. 2016; Mahdianpari et al. 2017; Thonfeld et al. 2020). In this algorithm, two important parameters are involved, namely, the maximum number of trees (*ntree*) and the number of split variables (*mtry*), and the reasonable selection for them is a hot issue in RF remote sensing classification. Some suggest that the default value of 500 for *ntree* is an acceptable value and *mtry* is set to the square root of the number of input variables (Lawrence et al. 2006; Ghosh and Joshi 2014; Belgiu and Drăguţ 2016). However, there are also some different opinions (Lou et al. 2020). In this study, different combinations of *ntree* and *mtry* parameters were designed to conduct the object-based RF model, in order to analyze their influence on the RF model construction. And the optimal RF models were chosen to classify the fuzing GE and UAV MSI.

RF can not only realize the remote sensing classification but also play an important role in feature dimensionality reduction and feature importance evaluation (Fu et al. 2017; Mahdianpari et al. 2017). RF is an ensemble classifier that creates the decision trees by drawing a subset of training samples through a bagging approach. Bootstrap self-help sampling is used to randomly select two-thirds of samples as a subset of training samples (in-bag samples) with the remaining one-third (out-of-the-bag (OOB) samples) are used in an internal cross-validation technique for estimating RF model performance (Belgiu and Drăguţ 2016). The OOB error generated by OOB samples can not only estimate the classification accuracy but also calculate the contribute of features to classification. And the feature importance estimation model is as follow (Zhang et al. 2019; Genuer et al. 2010; Fu et al. 2017):

$$VI(F_A) = \frac{1}{ntree}\sum_{t=1}^{ntree}\left(errOOB_{n_t}^{F_A} - errOOB_{Q_t}^{F_A}\right) \quad (1)$$

Where $VI$ is the variable importance, $F$ is the whole number of sample features, *ntree* is the number of decision trees, $errOOB_{Q_t}^{F_A}$ is the OOB error of the decision tree $t$ when no noise interference is added to any feature $F_A$, and $errOBB_{n_t}^{F_A}$ is the OOB error of the decision tree $t$ when noise interference is added to any feature $F_A$.

## Results and analysis

### Classification scenarios

In this study, three classification scenarios of different feature combination were designed for fuzing GE and UAV MSI, respectively, as shown in Table 5. The purposes of setting up different scenario for classification were as follows: (1) Analyzed the contribution of diffident features to object-based wetland classification. (2) Estimated the efforts of *ntree* and *mtry* on the accuracy of object-based RF model construction under different feature variables and images objects.

### RF parameters optimization

Through the corresponding algorithm improvement, different combinations of *ntree* and *mtry* parameters were set to optimize the object-based RF model for each GE and UAV classification scenario. And the final optimization results were shown in Figure 6 and Table 6. It was found that the fluctuation range of the training accuracy of object-based RF is about 2%-3% in each scenario. The training accuracy of the optimal models of each scenario reached over 85%. The RF parameters optimization results of fuzing GE and UAV MSI classification scenarios were consistent, this

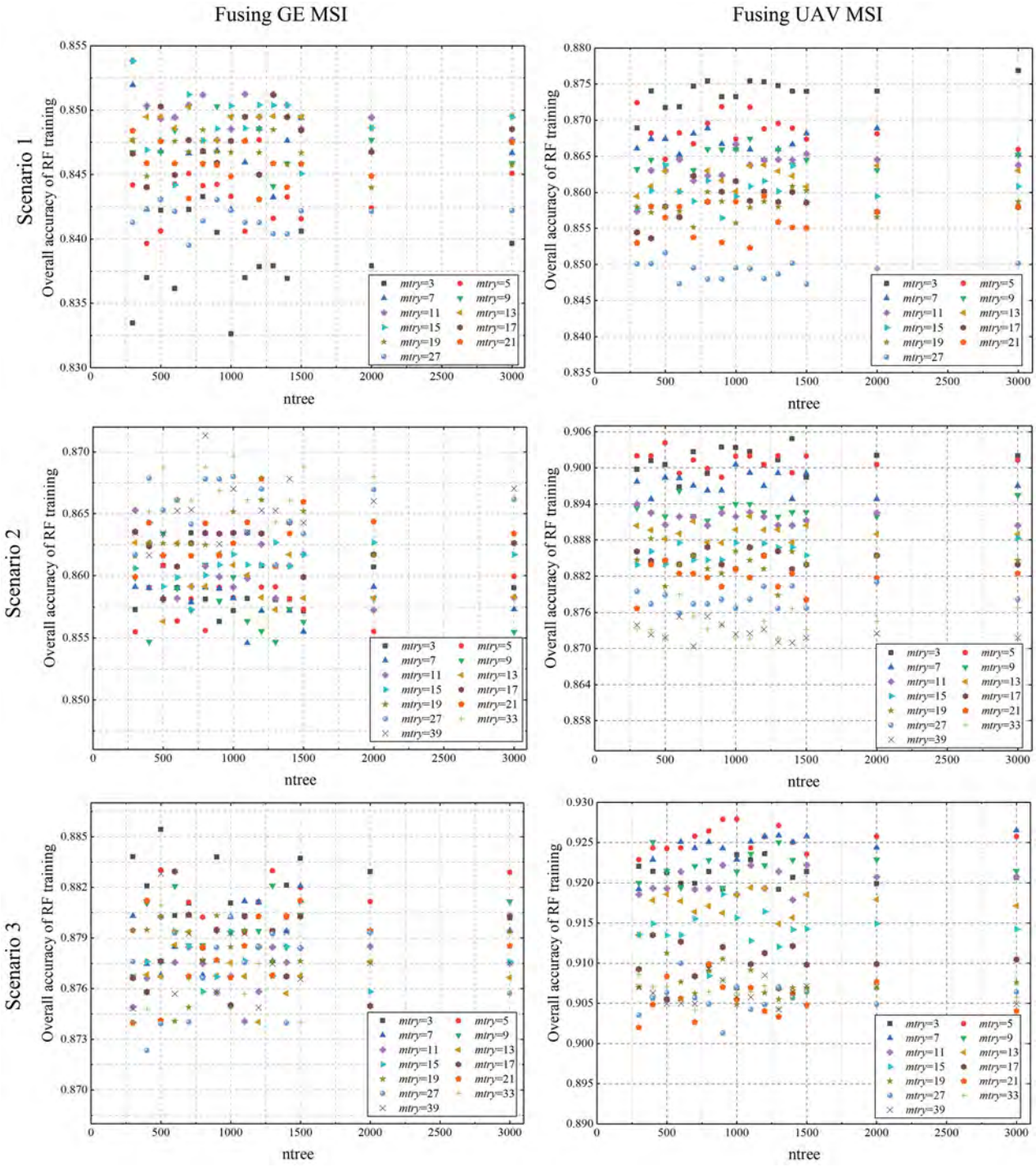


**Figure 6.** Object-based RF parameters (*ntree* and *mtry*) tuning of fuzing GE/UAV MSI.

is, the scenario 3 had a highest training overall accuracy, and the UAV scenario3 (0.9280) was higher than GE scenario3 (0.8854).

## *Classification results*

The three object-based RF classifications results with parameters (*ntree* and *mtry*) optimization for fuzing

**Table 6.** The optimal parameter of object-based RF model for fuzing GE/UAV MSI.

| | Selected features | *mtry* | *ntree* | Accuracy |
|---|---|---|---|---|
| GE Scenario1 | 33 | 11 | 300 | 0.8538 |
| GE Scenario2 | 57 | 39 | 800 | 0.8713 |
| GE Scenario3 | 76 | 3 | 500 | 0.8854 |
| UAV Scenario1 | 32 | 3 | 3000 | 0.8769 |
| UAV Scenario2 | 56 | 3 | 1400 | 0.9048 |
| UAV Scenario3 | 75 | 5 | 1000 | 0.9280 |

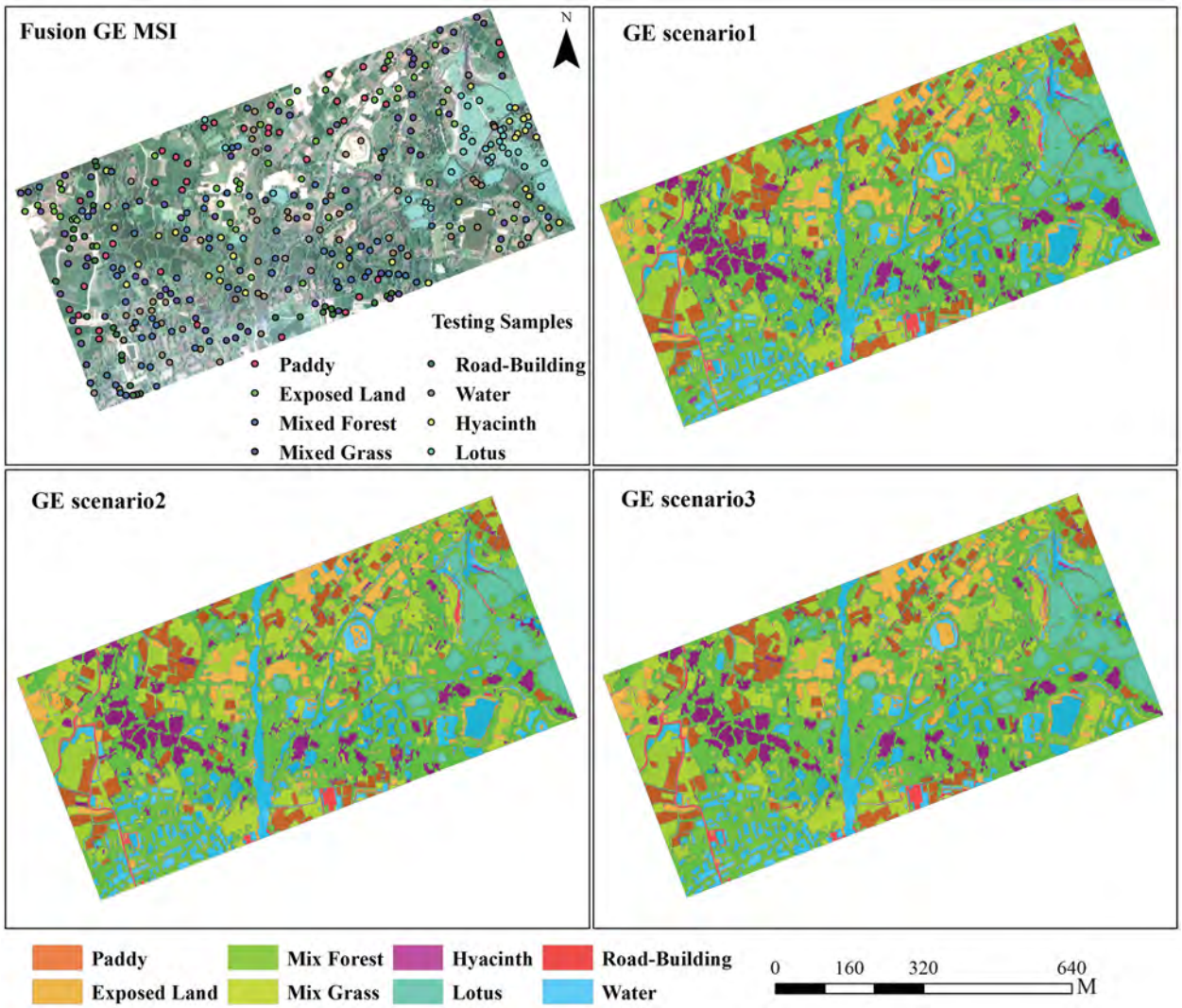


Figure 7. Classification results of fuzing GE MSI.

GE and UAV MSI can be seen in Figures 7 and 8, respectively. It was found that the wetland vegetation in this study area was well characterized, among which mixed forest and mixed grass accounted for the largest area. The mixed forest was mainly distributed around karst lakes and rivers, composed of *Linden*, *Bamboo* and *Paliurus*, mixed together. The current condition was not optimistic for Huixian Karst Wetland, which urgently needed the reasonable management and protection of human beings. The invasive species, named *Hyacinth*, had seriously affected the wetland ecological environment. However, the condition of the *Hyacinth* mixed with *Lotus* in the northeast was improved in 2019 (fusion GE MSI), compared with the condition in 2018 (fusion UAV MSI). But the *Hyacinth* growing in karst lakes in the southwest was still severe.

For the classification results of three GE scenarios, both GE scenario1 and 2 were relatively poor. For example, the exposed land in karst lakes in the northeast of the study area and the road-building in the southwest were not completely extracted in GE scenario1 and 2, and some small patches with mixed forest or mixed grassland were wrongly identified as *Hyacinth*. According to visual judgment and based on several field investigations, the GE scenario3 provided better performance.

For the classification results of three UAV scenarios, the phenomenon that the shadows were misidentified as water hyacinth was common, especially in the UAV scenario1. In UAV scenario1 and scenario 2, some exposed land objects in the northeast of study area were misidentified as road-building, and the extraction result for road-building in the south was

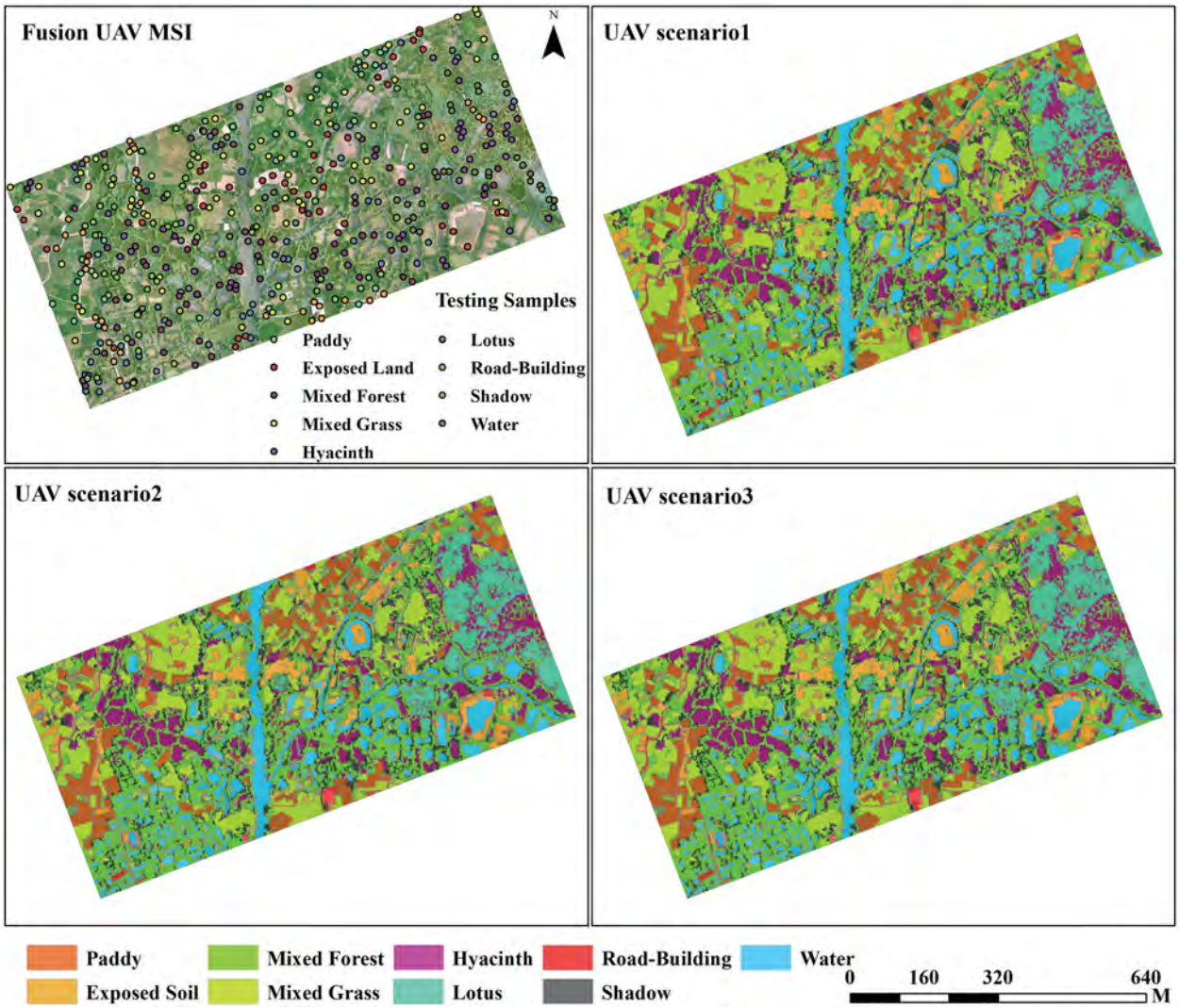


Figure 8. Classification results of fuzing UAV MSI.

incomplete. Therefore, the UAV scenario3 had better performance compared with the other two UAV scenarios.

### Accuracy assessment

To evaluate the classification scenarios combined with the multi-source feature combination and the optimized object-based RF algorithm, and to estimate the applicability of fuzing GE and UAV MSI in wetland finer classification, the accuracy of classification results was verified with the testing samples collected in the field, as shown in Table 7.

It was found that the UAV scenarios provided a higher classification accuracy compared with the corresponding GE scenarios, which is about 5%-7% higher on average. For instance, the GE scenario1, combined with the spectral and vegetation features, provided an OA of 82.53% (Kappa = 0.7966), while UAV scenario1 had an OA of 88.84% (Kappa = 0.873). On the basis of spectral features and vegetation indexes, GLCM texture and geometric and contextual features were considered respectively in classification scenarios, GE/UAV scenario2 and 3 showed relatively consistent regularity. The OA of GE/UAV sceanrio2 was improved by about 3% compared with scenario1 and 2% for GE/UAV sceanrio3 compared with scenario2. The highest classification accuracy of fuzing GE/UAV MSI was achieved in scenario3. The OA of GE scenario3 was 87.37% (Kappa = 0.8528), while UAV scenario3 was 94.31% (Kappa = 0.9353).

Although the OA and Kappa were improved from GE/UAV scenario1 to scenario3, there was a great difference for the UA and PA of single vegetation type in classification. Not all of them showed an increasing tendency, and the classification accuracy of a few

**Table 7.** Three different feature combination classification scenarios are constructed for fusion GE and UAV MSI, respectively, based on selected features. [Trois scénarios différents de classification des combinaisons de fonctionnalités sont construits pour la fusion GE et UAV MSI, respectivement, en fonction de fonctionnalités sélectionnées.]

| | GE Scenario1 | | GE Scenario2 | | GE Scenario3 | | UAV Scenario1 | | UAV Scenario2 | | UAV Scenario3 | |
|---|---|---|---|---|---|---|---|---|---|---|---|---|
| | UA/% | PA/% | UA/% | PA/% | UA/% | PA/% | UA/% | PA/% | UA/% | PA/% | UA/% | PA/% |
| Paddy | 92.1 | 89.7 | 91.9 | 87.2 | 92.1 | 89.7 | 88.9 | 90.9 | 91.1 | 93.3 | 100 | 93.2 |
| Exposed land | 91.3 | 87.5 | 91.5 | 89.6 | 90 | 93.8 | 89.6 | 95.6 | 89.4 | 93.3 | 91.7 | 97.8 |
| Mixed forest | 77 | 81.4 | 82.1 | 91.4 | 82.9 | 97.1 | 78.8 | 94 | 85.9 | 95.2 | 91.7 | 92.8 |
| Mixed grass | 77.3 | 86.6 | 81.3 | 91 | 87.7 | 85.1 | 86 | 65.2 | 93 | 80.3 | 89.4 | 89.4 |
| Hyacinth | 68.2 | 48.4 | 80 | 51.6 | 89.5 | 54.8 | 94.1 | 78 | 94.6 | 85.4 | 92.7 | 92.7 |
| Lotus | 93.3 | 87.5 | 93.1 | 84.4 | 96.7 | 90.6 | 92.3 | 97.3 | 91.9 | 91.9 | 94.4 | 91.9 |
| Road-building | 97.5 | 93.3 | 87.9 | 96.7 | 90.3 | 93.3 | 97 | 86.5 | 91.4 | 86.5 | 100 | 91.9 |
| Water | 80 | 80 | 83 | 80 | 80.7 | 83.6 | 96.2 | 96.2 | 98.1 | 100 | 98.1 | 100 |
| Shadow | – | | – | | – | | 91.2 | 100 | 96.3 | 100 | 96.3 | 100 |
| OA/% | 82.53 | | 85.48 | | 87.37 | | 88.84 | | 91.90 | | 94.31 | |
| Kappa | 0.7966 | | 0.8308 | | 0.8528 | | 0.873 | | 0.9079 | | 0.9353 | |

The object-based random forest (RF) algorithms with parameters (*mtry* and *ntree*) optimization are used to carry out finer wetland classification. Results show that the fusion GE and UAV MSI have good applicability in the finer wetland classification, especially the fusion UAV images, and integrating multi-source features could improve classification accuracy. Both data sources reach the highest accuracy in scenario3. The overall accuracy of fusion UAV image scenario3 is 94.31% (Kappa = 0.9353), and that of fusion GE image scenario3 is 87.37% (Kappa = 0.8528). The contribution of different features to wetland classification is obtained with spectral and vegetation indexes>texture features>geometric and contextual features. [Les algorithmes de forêt aléatoire (RF) basés sur des objets avec optimization des paramètres (*mtry* et *ntree*) sont utilisés pour effectuer une classification plus fine des zones humides. Les résultats montrent que la fusion GE et UAV MSI ont une bonne applicabilité dans la classification plus fine des zones humides, en particulier les images uav fusion, et l'intégration de fonctionnalités multi-sources pourrait améliorer la précision de classification. Les deux sources de données atteignent la plus grande précision dans le scénario3. La précision globale du scénario d'image uav fusion3 est de 94,31% (Kappa = 0,9353), et celle du scénario d'image GE fusion3 est de 87,37% (Kappa = 0,8528). La contribution de différentes caractéristiques à la classification des milieux humides est obtenue à l'aide d'indices spectraux et de végétation > expéciations detexture > géométriques et contextuelles.of GE/UAV classification accuracy.]

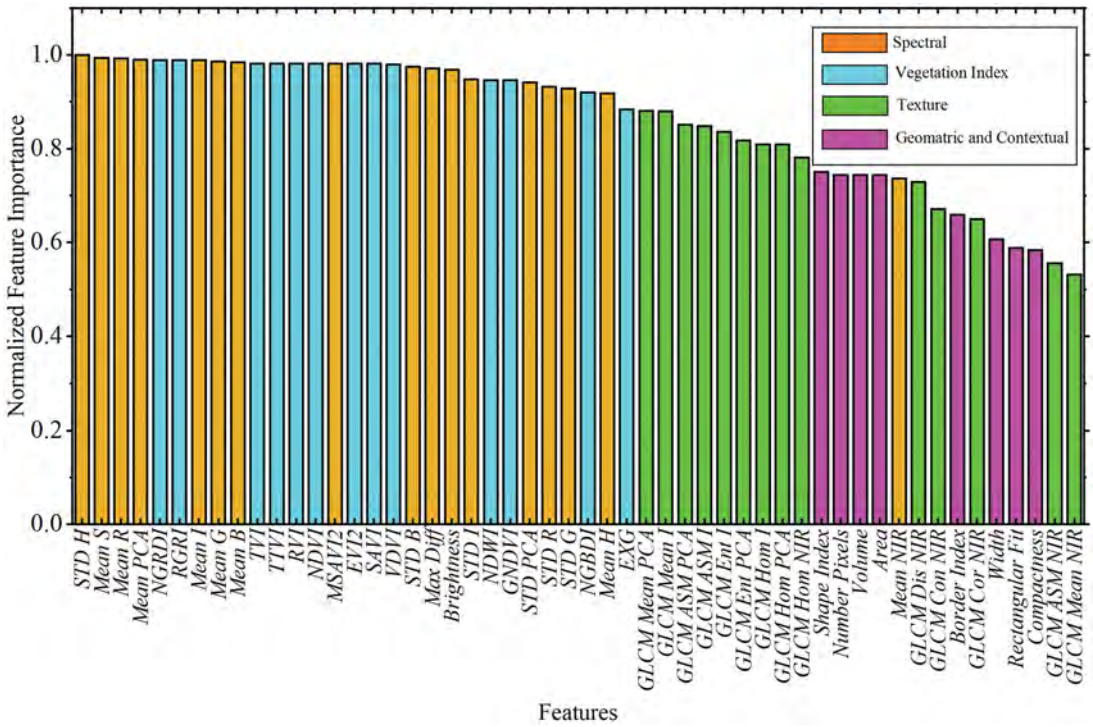


**Figure 9.** The feature importance distribution of GE scenario3 (features that the score greater than 0.5 were selected).

single vegetation type was reduced. For example, the UA and PA of mixed forest, mixed grass and hyacinth were improved while those of lotus were decreased from GE/UAV scenario1 to scenario2. From UAV scenario2 to scenario3, the UA of hyacinth and mixed grass were also decreased.

### *Feature importance evaluation*

The feature importance estimation participating in GE and UAV classification scenario3 was carried out based on RF algorithm, and the results were normalized, as shown in Figures 9 and 10 (features that the score greater than 0.5 were selected). On the whole,

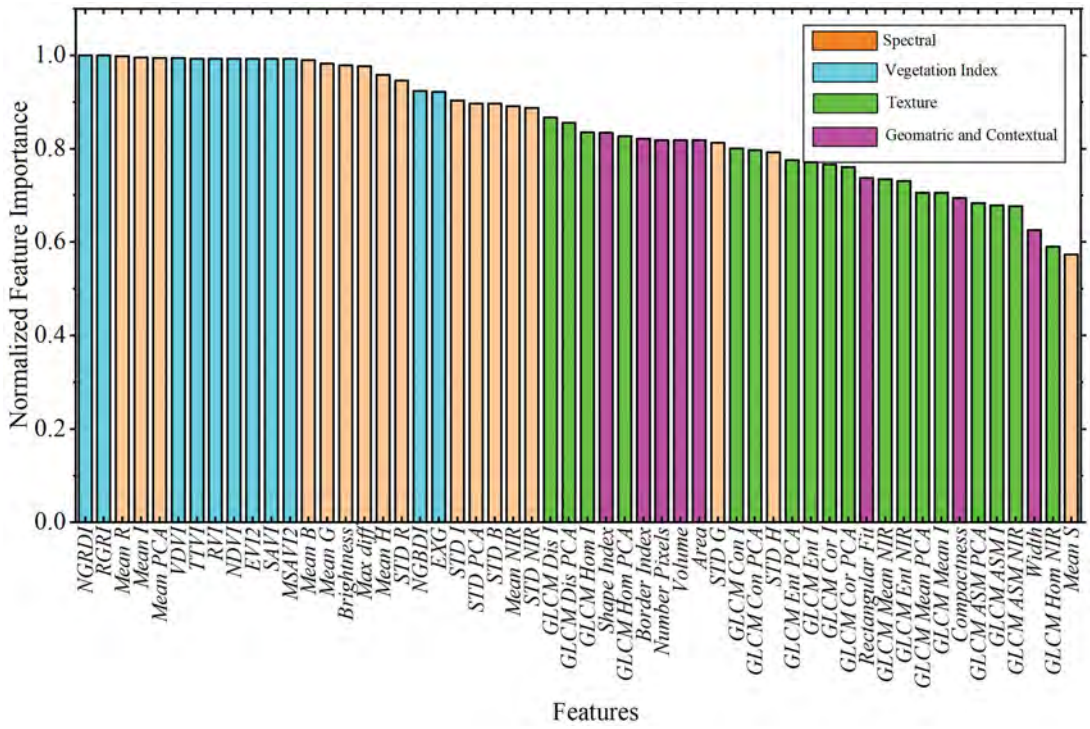


**Figure 10.** The feature importance distribution of UAV scenario3 (features that the score greater than 0.5 were selected).

the feature importance scores of GE and UAV scenaro3 showed a relatively consistent result, this is, spectral feature and vegetation index scored the highest, followed by texture feature, and finally geometric and contextual feature. Specific to local analysis, it was found that the importance of spectral features of fusion NIR band was lower than other spectral features. The texture feature scores of GE and UAV scenario3 were quite different, but the entropy and homogeneity texture features calculated from GLCM showed a high importance in both datasets. In addition, the texture features based on PCA and I were more important than those extracted from NIR bands. For vegetation indexes, NGBDI and RGRI showed high importance in both fuzing GE and UAV feature datasets. Among the geometric and contextual features, polarization was very serious. The importance of border index, shape index, number of pixels and volume were relatively high compared with the other geometric and contextual features.

## Discussion

Wetland vegetation types are complex and the spectrum confusion is serious. Finer classification of small-scale wetland using GE and UAV RGB images has obvious limitations, which makes it difficult to provide reasonable identification accuracy. And the classification scheme with medium resolution Landsat-8 or Sentinel-2 is limited by poor spatial resolution. Therefore, GE/UAV images and Sentinel-2A were fused with GS transformation to obtain ultra-high spatial resolution MSI. NDVI and NDWI were calculated based on fuzing GE and UAV MSI, and both of them could better represent the different vegetation types in wetlands (Figure 4). The difference between non-vegetation and vegetation was obvious, which was helpful to realize the finer and high precision classification. In addition, object-based RF algorithm was chosen to explore the applicability of fuzing GE and UAV MSI in finer small-scale wetland classification with high precision, in order to avoid the influence of "salt and pepper" in pixel-based classification for ultra-high spatial resolution images.

The *shape* and *compactness* parameters of FNEA MRS were selected by trial-and-error fashion. By analyzing those results, it was found that the change of *shape* parameter was more sensitive to the quality of the FNEA MRS results compared with *compactness* index, and setting a smaller *shape* parameter was easier to obtain the ideal segmentation results, which was also consistent with the results obtained by Whyte et al (2018). The subjective intervention of human was avoided as far as possible when selecting the *scale* index suitable for FNEA MRS. The ESP2 tool was used for iterative segmentation, which relies on the potential of local variance (LV) to detect scale transformations in geospatial data. This tool is so popular

and has a good applicability in *scale* parameter selection in object-based classification (Tian et al. 2020; Belgiu and Drăguţ 2014). But it is only a semi-automatic scale parameter selection tool. The local variance curve will be very gentle and the inflection point is not obvious when the segmentation initial parameters are set unreasonably. And it needs to reset the parameters for iterative segmentation. During the FNEA MRS process, the RGRI and I bands were involved and given higher weighting in addition to the RGB bands of fuzing GE and UAV MSI. In this way, better segmentation results could be obtained. The exposed land, hyacinth and paddy of fuzing GE and UAV MSI had high homogeneity, and its segmented objects of FNEA MRS were more orderly and smoother. However, lotus and mixed forest had high heterogeneity, and the large number of fragmented patches posed a challenge to the finer and high precision classification, as shown in Figure 5.

By analyzing the optimal parameters (*ntree* and *mtry*) of object-based RF model training (Table 6), it was found that they were not consistent with the publishing opinions that setting *ntree* as 500 and *mtry* as the square root of input variables could provide better RF model construction accuracy (Lawrence et al. 2006; Ghosh and Joshi 2014; Belgiu and Drăguţ 2016). The optimal *ntree* parameter for fuzing UAV MSI was generally larger than that for GE images, while the optimal *mtry* parameter was smaller than that for fuzing GE MSI. Therefore, it could infer that the optimal *mtry* and *ntree* parameters may be related to the number of image objects of FNEA MRS in object-based RF model training.

Due to higher image quality (spatial resolution, texture and geometric features) for the fuzing UAV MSI, its extracted classification features were better than fuzing GE image. The final feature extraction and classification in OBIA is highly dependent on the quality of image segmentation. After the FNEA MRS process, the segmentation result of fuzing UAV image was better, which can define vegetation boundary and expressing wetland scattered patches more accurately. And under the optimal segmentation parameter condition, the fuzing GE image had 4,260 segmentation objects while 9,282 objects were obtained for the fuzing UAV image. Thus, the classification accuracy of UAV scenarios was better than that of GE scenarios, which indicated that fuzing UAV MSI was more suitable for finer small-scale wetland classification, compared with fuzing GE MSI. Spectral features and vegetation indexes are the most widely used in wetland vegetation classification (Rampi et al. 2014; Dronova 2015). Both fuzing GE and UAV MSI achieved OA of over 80% in scenario1, respectively, only spectral and vegetation features were involved. In addition, it was found that the scores of spectral and vegetation indexes were the highest when analyzing the estimation results of feature contribution (Figures 9 and 10), which also showed the necessity of increasing the spectral resolution of GE and UAV RGB images in this study. Texture features were also widely used, while geometric and contextual features were less used than others (Dronova 2015). The OA and Kappa were significantly improved when considering the texture feature, geometric and contextual features on the basis of GE/UAV scenario1. And the accuracy improvement of scenario2 was higher than that of scenario3 (Table 7), indicating that texture features were more important than geometric and contextual features, which could also be verified from the evaluation results of feature importance. Although the scenario that combined the multi-source features could provide a higher OA, the UA and PA of single vegetation type varied greatly. For example, the classification accuracy of lotus and road-building had a tendency of decrease when adding texture feature to GE/UAV scenaro1. Therefore, it was necessary to reasonably chose the features used in classification scenario based on the characteristics of the ground objects.

By analyzing the feature importance evaluation results (Figures 9 and 10), it was found that the results of fuzing GE and UAV MSI showed consistent regularity with spectral and vegetation features > texture features > geometric and contextual features. The contribution of spectral and texture features of PCA and I bands were significantly higher than those of NIR band, which may be related to the quality of fuzing images. The geometric and contextual feature importance were seriously differentiated in the two datasets. There were only eight variables with importance scores greater than 0.5 (8/19). Therefore, geometric and contextual features cannot be blindly added when selecting feature variables using object-based classification. There were also local differences for the GE and UAV feature importance. Dissimilarity texture scored higher in UAV scenario3 feature dataset, but it did not appear in the feature importance distribution of GE scenario3 shown in Figure 9. The GE and UAV scenario3 differed in the importance of texture features, which was related to the image quality and resolution to some extent. The spatial resolution of UAV image was higher than GE image, and the heterogeneity of mixed forest and lotus was higher

in fuzing UAV MSI, which resulted in the difference of texture feature importance in two datasets.

In addition, there were some uncertainties in GE and UAV classification scenarios. The vegetation types of mixed forest and mix grass were complex. Among them, the mixed forest was mainly composed of *Linden*, *Bamboo* and *Paliurus*, while the mixed grass consisted of *Bermuda grass*, *Eleusine indica* and *Ditch millet*, mixed together. It was difficult to further distinguish them using fuzing GE and UAV MSI. Therefore, they were classified as a vegetation cluster in this study respectively, named mixed forest and mixed grass. High spatial resolution images were easily affected by the shadows of ground object, which was particularly obvious in low-altitude UAV images of this study. And the shadows were classified into a separate class for each UAV classification scenario. According to the statistical result, the shadow area of UAV scenario3 was about 47,972 $m^2$, covering mainly mixed forest and grass near the forest. As a result, mixed forest and mixed grass areas were smaller than they really one in UAV classification scenarios. The shadows also caused some *Hyacinth* to be misclassified, especially in GE/UAV scenario1. And this phenomenon had been improved to a certain extent when combining multi-source variables in classification scheme.

## Conclusion

In this study, the fusion of GE and Sentienl-2A image, fusion of UAV and Sentinel-2A image and optimized object-based RF algorithm with multi-source feature combination are used to carry out finer small-scale wetland classification. The main conclusions are summarized as follows: (1) The fuzing GE and UAV MSI has good applicability in finer small-scale wetland classification. The wetland vegetation and invasive species named *Hyacinth* are accurately extracted, and the classification accuracy could be improved by integrating multi-source features using in classification scenario. The overall accuracy of GE scenario3 and UAV scenario3 is 87.83% and 94.31% respectively, suggesting that the fuzing UAV MSI is better than fuzing GE MSI in finer small-scale wetland classification. (2) In FNEA MRS of object-based finer wetland classification, the *shape* parameter is more sensitive to image segmentation results compared with *compactness* parameter. A small *shape* parameter possibly provided a reasonable segmentation result. In addition to the original spectral bands, other image layers could be added to optimize the FNEA MRS result, such as vegetation indexes. (3) the size of *ntree* and *mtry* parameters may be related to the number of segmented image objects in object-based RF model construction. The more image objects there are, the larger the optimal *ntree* parameter will be, while the *mtry* parameter will be smaller. (4) The contribution of different variables using in wetland classification scenario is obtained with spectral and vegetation indexes > texture features > geometric and contextual features.

The high spatial resolution images released by GE have low temporal resolution, while the fluctuation of wetland water level will cause rapid and frequent changes of vegetation cover type, spatial distribution and density. In the future, the finer dynamic monitoring of wetland vegetation requires the multi-source high resolution remote sensing data, and the GE images can be used as a supplement. In addition, GE/UAV images fused with Sentinel-2A data only provided vegetation cluster level classification in this study. It was necessary to combine the UAV 3 D point clouds or hyperspectral data to achieve further classification.

## Acknowledgments

The authors would like to thank the anonymous reviewers and the editor for their constructive comments and suggestions.

## Disclosure statement

No potential conflict of interest was reported by the author(s).

## Funding

This work was supported by the strategic priority research program project of the Chinese Academy of Sciences [grant number XDA23040100]; Jiangsu Province Distinguished Professor Project [grant number R2018T20] and Startup Foundation for Introducing Talent of NUIST.

## ORCID

Shuanggen Jin http://orcid.org/0000-0002-5108-4828

## References

Alvarez-Vanhard, E., Houet, T., Mony, C., Lecoq, L., and Corpetti, T. 2020. "Can UAVs fill the gap between in situ surveys and satellites for habitat mapping." *Remote Sensing of Environment*, Vol. 243: pp. 111780. doi:10.1016/j.rse.2020.111780.

Anderson, K., and Gaston, K.J. 2013. "Lightweight unmanned aerial vehicles will revolutionize spatial ecology." *Frontiers in Ecology and the Environment*, Vol. 11(No. 3): pp. 138–146. doi:10.1890/120150.

Alvarez-Cobelas, M., Sánchez-Carrillo, S., Cirujano, S., and Angeler, D.G. 2007. "Long-term changes in spatial patterns of emergent vegetation in a Mediterranean floodplain: Natural versus anthropogenic constraints." *Plant Ecology*, Vol. 194(No. 2): pp. 257–271. doi:10.1007/s11258-007-9289-6.

Abeysinghe, T., Simic Milas, A., Arend, K., Hohman, B., Reil, P., Gregory, A., and Vázquez-Ortega, A. 2019. "Mapping invasive phragmites australis in the old woman creek estuary using UAV remote sensing and machine learning classifiers." *Remote Sensing*, Vol. 11(No. 11): pp. 1380. doi:10.3390/rs11111380.

Brook, A., De Micco, V., Battipaglia, G., Erbaggio, A., Ludeno, G., Catapano, I., and Bonfante, A. 2020. "A smart multiple spatial and temporal resolution system to support precision agriculture from satellite images: Proof of concept on Aglianico vineyard." *Remote Sensing of Environment*, Vol. 240: pp. 111679. doi:10.1016/j.rse.2020.111679.

Belgiu, M., and Drăguţ, L. 2016. "Random forest in remote sensing: A review of applications and future directions." *ISPRS Journal of Photogrammetry and Remote Sensing*, Vol. 114: pp. 24–31. doi:10.1016/j.isprsjprs.2016.01.011.

Blaschke, T. 2010. "Object based image analysis for remote sensing." *ISPRS Journal of Photogrammetry and Remote Sensing*, Vol. 65(No. 1): pp. 2–16. doi:10.1016/j.isprsjprs.2009.06.004.

Bendig, J., Yu, K., Aasen, H., Bolten, A., Bennertz, S., Broscheit, J., Gnyp, M.L., and Bareth, G. 2015. "Combining UAV-based plant height from crop surface models, visible, and near infrared vegetation indices for biomass monitoring in barley." *International Journal of Applied Earth Observation and Geoinformation*, Vol. 39: pp. 79–87. doi:10.1016/j.jag.2015.02.012.

Belgiu, M., and Drăguţ, L. 2014. "Comparing supervised and unsupervised multiresolution segmentation approaches for extracting buildings from very high resolution imagery." *ISPRS Journal of Photogrammetry and Remote Sensing*, Vol. 96: pp. 67–75. doi:10.1016/j.isprsjprs.2014.07.002.

Breiman, L. 1996. "Bagging predictors." *Machine Learning*, Vol. 24(No. 2): pp. 123–140. doi:10.1007/BF00058655.

Breiman, L. 2001. "Random forests." *Machine Learning*, Vol. 45(No. 1): pp. 5–32. doi:10.1023/A:1010933404324.

Chen, Y., He, X., Xu, J., Zhang, R., and Lu, Y. 2020. "Scattering feature set optimization and polarimetric SAR classification using object-oriented RF-SFS algorithm in coastal wetlands." *Remote Sensing*, Vol. 12(No. 3): pp. 407. doi:10.3390/rs12030407.

Cao, J., Leng, W., Liu, K., Liu, L., He, Z., and Zhu, Y. 2018. "Object-based mangrove species classification using unmanned aerial vehicle hyperspectral images and digital surface models." *Remote Sensing*, Vol. 10(No. 2): pp. 89. doi:10.3390/rs10010089.

Clark, M.L., Aide, T.M., Grau, H.R., and Riner, G. 2010. "A scalable approach to mapping annual land cover at 250 m using MODIS time series data: A case study in the Dry Chaco ecoregion of South America." *Remote Sensing of Environment*, Vol. 114(No. 11): pp. 2816–2832. doi:10.1016/j.rse.2010.07.001.

Canisius, F., Turral, H., and Mbilinyi, B.P. 2011. "Analysis of seasonal land use in Usangu wetlands, Tanzania: An object-oriented technique for multi-temporal analysis with high-resolution data." *International Journal of Remote Sensing*, Vol. 32(No. 7): pp. 1885–1900. doi:10.1080/01431161003639645.

de Almeida Furtado, L.F., Silva, T.S.F., and de Moraes Novo, E.M.L. 2016. "Dual-season and full-polarimetric C band SAR assessment for vegetation mapping in the Amazon várzea wetlands." *Remote Sensing of Environment*, Vol. 174: pp. 212–222. doi:10.1016/j.rse.2015.12.013.

Davidson, N.C. 2014. "How much wetland has the world lost? Long-term and recent trends in global wetland area." *Marine and Freshwater Research*, Vol. 65(No. 10): pp. 934–941. doi:10.107/MF14173.

Duro, D.C., Franklin, S.E., and Dubé, M.G. 2012. "A comparison of pixel-based and object-based image analysis with selected machine learning algorithms for the classification of agricultural landscapes using SPOT-5 HRG imagery." *Remote Sensing of Environment*, Vol. 118: pp. 259–272. doi:10.1016/j.rse.2011.11.020.

Dronova, I. 2015. "Object-based image analysis in wetland research: A review." *Remote Sensing*, Vol. 7(No. 5): pp. 6380–6413. doi:10.3390/rs70506380.

Drăguţ, L., Csillik, O., Eisank, C., and Tiede, D. 2014. "Automated parameterisation for multi-scale image segmentation on multiple layers." *ISPRS Journal of Photogrammetry and Remote Sensing*, Vol. 88(No. 100): pp. 119–127. doi:10.1016/j.isprsjprs.2013.11.018.

Drăguţ, L., Tiede, D., and Levick, S.R. 2010. "ESP: A tool to estimate scale parameter for multiresolution image segmentation of remotely sensed data." *International Journal of Geographical Information Science*, Vol. 24(No. 6): pp. 859–871. doi:10.1080/13658810903174803.

Fu, B., Wang, Y., Campbell, A., Li, Y., Zhang, B., Yin, S., Xing, Z., and Jin, X. 2017. "Comparison of object-based and pixel-based Random Forest algorithm for wetland vegetation mapping using high spatial resolution GF-1 and SAR data." *Ecological Indicators*, Vol. 73: pp. 105–117. doi:10.1016/j.ecolind.2016.09.029.

Guo, Z., Shao, X., Xu, Y., Miyazaki, H., Ohira, W., and Shibasaki, R. 2016. "Identification of village building via Google Earth images and supervised machine learning methods." *Remote Sensing*, Vol. 8(No. 4): pp. 271. doi:10.3390/rs8040271.

Genuer, R., Poggi, J.M., and Tuleau-Malot, C. 2010. "Variable selection using random forests." *Pattern Recognition Letters*, Vol. 31(No. 14): pp. 2225–2236. doi:10.1016/j.patrec.2010.03.014.

Ghosh, A., and Joshi, P.K. 2014. "A comparison of selected classification algorithms for mapping bamboo patches in lower Gangetic plains using very high resolution WorldView 2 imagery." *International Journal of Applied Earth Observation and Geoinformation*, Vol. 26: pp. 298–311. doi:10.1016/j.jag.2013.08.011.

Huang, M., Chen, N., Du, W., Chen, Z., and Gong, J. 2018. "DMBLC: An indirect urban impervious surface area extraction approach by detecting and masking

background land cover on Google Earth Image." *Remote Sensing*, Vol. 10(No. 5): pp. 766. doi:10.3390/rs10050766.

Hu, Q., Wu, W., Xia, T., Yu, Q., Yang, P., Li, Z., and Song, Q. 2013. "Exploring the use of Google Earth imagery and object-based methods in land use/cover mapping." *Remote Sensing*, Vol. 5(No. 11): pp. 6026–6042. doi:10.3390/rs5116026.

Hossain, M.D., and Chen, D. 2019. "Segmentation for object-based image analysis (OBIA): A review of algorithms and challenges from remote sensing perspective." *ISPRS Journal of Photogrammetry and Remote Sensing*, Vol. 150: pp. 115–134. doi:10.1016/j.isprsjprs.2019.02.009.

Ji, W., Xu, X., and Murambadoro, D. 2015. "Understanding urban wetland dynamics: Cross-scale detection and analysis of remote sensing." *International Journal of Remote Sensing*, Vol. 36(No. 7): pp. 1763–1788. doi:10.1080/01431161.2015.1024895.

Jenerowicz, A., and Woroszkiewicz, M. 2016. "The pan-sharpening of satellite and UAV imagery for agricultural applications." In SPIE Remote Sensing; International Society for Optics and Photonics: Bellingham, WA, USA, October 9998, p. 99981S. doi:10.1117/12.2241645.

Kaimaris, D., Georgoula, O., Patias, P., and Stylianidis, E. 2011. "Comparative analysis on the archaeological content of imagery from Google Earth." *Journal of Cultural Heritage*, Vol. 12(No. 3): pp. 263–269. doi:10.1016/j.culher.2010.12.007.

Lawrence, R.L., Wood, S.D., and Sheley, R.L. 2006. "Mapping invasive plants using hyperspectral imagery and Breiman Cutler classifications (RandomForest)." *Remote Sensing of Environment*, Vol. 100(No. 3): pp. 356–362. doi:10.1016/j.rse.2005.10.014.

Lv, J., Jiang, W., Wang, W., Wu, Z., Liu, Y., Wang, X., and Li, Z. 2019. "Wetland loss identification and evaluation based on landscape and remote sensing indices in Xiong'an new area." *Remote Sensing*, Vol. 11(No. 23): pp. 2834. doi:10.3390/rs11232834.

Lou, P., Fu, B., He, H., Li, Y., Tang, T., Lin, X., Fan, D., and Gao, E. 2020. "An optimized object-based random forest algorithm for marsh vegetation mapping using high-spatial-resolution GF-1 and ZY-3 data." *Remote Sensing*, Vol. 12(No. 8): pp. 1270. doi:10.3390/rs12081270.

Li, D., and Li, M. 2014. "Research advance and application prospect of unmanned aerial vehicle remote sensing system." *Geomatics and Information Science of Wuhan University*, Vol. 39(No. 5): pp. 505–513. doi:10.13203/j.whugis20140045.

Lu, D., Li, G., Moran, E., Dutra, L., and Batistella, M. 2014. "The roles of textural images in improving land-cover classification in the Brazilian Amazon." *International Journal of Remote Sensing*, Vol. 35(No. 24): pp. 8188–8207. doi:10.1080/01431161.2014.980920.

Mahdavi, S., Salehi, B., Amani, M., Granger, J.E., Brisco, B., Huang, W., and Hanson, A. 2017. "Object-based classification of wetlands in Newfoundland and Labrador using multi-temporal PolSAR data." *Canadian Journal of Remote Sensing*, Vol. 43(No. 5): pp. 432–450. doi:10.1080/07038992.2017.1342206.

Mahdianpari, M., Salehi, B., Mohammadimanesh, F., Brisco, B., Homayouni, S., Gill, E., DeLancey, E.R., and Bourgeau-Chavez, L. 2020. "Big data for a big country: The first generation of canadian wetland inventory map at a spatial resolution of 10-m using Sentinel-1 and Sentinel-2 data on the Google Earth engine cloud computing platform." *Canadian Journal of Remote Sensing*, Vol. 46(No. 1): pp. 15–33. doi:10.1080/07038992.2019.1711366.

Mahdianpari, M., Salehi, B., Mohammadimanesh, F., and Motagh, M. 2017. "Random forest wetland classification using ALOS-2 L-band, RADARSAT-2 C-band, and TerraSAR-X imagery." *ISPRS Journal of Photogrammetry and Remote Sensing*, Vol. 130: pp. 13–31. doi:10.1016/j.isprsjprs.2017.05.010.

Mering, C., Baro, J., and Upegui, E. 2010. "Retrieving urban areas on Google Earth images: Application to towns of West Africa." *International Journal of Remote Sensing*, Vol. 31(No. 22): pp. 5867–5877. doi:10.1080/01431161.2010.512311.

Ma, L., Li, M., Ma, X., Cheng, L., Du, P., and Liu, Y. 2017. "A review of supervised object-based land-cover image classification." *ISPRS Journal of Photogrammetry and Remote Sensing*, Vol. 130: pp. 277–293. doi:10.1016/j.isprsjprs.2017.06.001.

Mingwu, Z., Haijiang, J., Desuo, C., and Chunbo, J. 2010. "The comparative study on the ecological sensitivity analysis in Huixian karst wetland." *Procedia Environmental Sciences*, Vol. 2: pp. 386–398. doi:10.1016/j.proenv.2010.10.043.

Mhangara, P., Mapurisa, W., and Mudau, N. 2020. "Comparison of image fusion techniques using Satellite Pour l'Observation de la Terre (SPOT) 6 satellite imagery." *Applied Sciences*, Vol. 10(No. 5): pp. 1881. doi:10.3390/app10051881.

Moffett, K.B., and Gorelick, S.M. 2013. "Distinguishing wetland vegetation and channel features with object-based image segmentation." *International Journal of Remote Sensing*, Vol. 34(No. 4): pp. 1332–1354. doi:10.1080/01431161.2012.718463.

Pulighe, G., Baiocchi, V., and Lupia, F. 2016. "Horizontal accuracy assessment of very high resolution Google Earth images in the city of Rome, Italy." *International Journal of Digital Earth*, Vol. 9(No. 4): pp. 342–362. doi:10.1080/17538947.2015.1031716.

Powers, R.P., Hay, G.J., and Chen, G. 2012. "How wetland type and area differ through scale: A GEOBIA case study in Alberta's Boreal Plains." *Remote Sensing of Environment*, Vol. 117: pp. 135–145. doi:10.1016/j.rse.2011.07.009.

Pande-Chhetri, R., Abd-Elrahman, A., Liu, T., Morton, J., and Wilhelm, V.L. 2017. "Object-based classification of wetland vegetation using very high-resolution unmanned air system imagery." *European Journal of Remote Sensing*, Vol. 50(No. 1): pp. 564–576. doi:10.1080/22797254.2017.1373602.

Rampi, L.P., Knight, J.F., and Pelletier, K.C. 2014. "Wetland mapping in the Upper Midwest United States." *Photogrammetric Engineering & Remote Sensing*, Vol. 80(No. 5): pp. 439–448. doi:10.14358/PERS.80.5.439.

Szantoi, Z., Escobedo, F.J., Abd-Elrahman, A., Pearlstine, L., Dewitt, B., and Smith, S. 2015. "Classifying spatially heterogeneous wetland communities using machine learning algorithms and spectral and textural features."

*Environmental Monitoring and Assessment*, Vol. 187(No. 5): pp. 262. doi:10.1007/s10661-015-4426-5.

Tao, Z., Jun, L., Keming, Y., Wenshan, L., and Yuyu, Z. 2015. "Fusion Algorithm for hyperspectral remote sensing image combined with harmonic analysis and Gram-Schmidt transform." *Acta Geodaetica et Cartographica Sinica*, Vol. 44(No. 9): pp. 1042. doi:10.11947/j.AGCS.2015.20140637.

Thonfeld, F., Steinbach, S., Muro, J., and Kirimi, F. 2020. "Long-term land use/land cover change assessment of the Kilombero catchment in Tanzania using random forest classification and robust change vector analysis." *Remote Sensing*, Vol. 12(No. 7): pp. 1057. doi:10.3390/rs12071057.

Tian, Y., Jia, M., Wang, Z., Mao, D., Du, B., and Wang, C. 2020. "Monitoring invasion process of Spartina alterniflora by seasonal Sentinel-2 imagery and an object-based random forest classification." *Remote Sensing*, Vol. 12(No. 9): pp. 1383. doi:10.3390/rs12091383.

Whyte, A., Ferentinos, K.P., and Petropoulos, G.P. 2018. "A new synergistic approach for monitoring wetlands using Sentinels-1 and 2 data with object-based machine learning algorithms." *Environmental Modelling & Software*, Vol. 104: pp. 40–54. doi:10.1016/j.envsoft.2018.01.023.

Wang, X., Gao, X., Zhang, Y., Fei, X., Chen, Z., Wang, J., Zhang, Y., Lu, X., and Zhao, H. 2019. "Land-Cover classification of coastal wetlands using the RF algorithm for Worldview-2 and Landsat 8 images." *Remote Sensing*, Vol. 11(No. 16): pp. 1927. doi:10.3390/rs11161927.

Watts, A.C., Ambrosia, V.G., and Hinkley, E.A. 2012. "Unmanned aircraft systems in remote sensing and scientific research: Classification and considerations of use." *Remote Sensing*, Vol. 4(No. 6): pp. 1671–1692. doi:10.3390/rs4061671.

Xiao, H., Shahab, A., Li, J., Xi, B., Sun, X., He, H., and Yu, G. 2019. "Distribution, ecological risk assessment and source identification of heavy metals in surface sediments of Huixian karst wetland, China." *Ecotoxicology and Environmental Safety*, Vol. 185: pp. 109700. doi:10.1016/j.ecoenv.2019.109700.

Yu, L., and Gong, P. 2012. "Google Earth as a virtual globe tool for Earth science applications at the global scale: Progress and perspectives." *International Journal of Remote Sensing*, Vol. 33(No. 12): pp. 3966–3986. doi:10.1080/01431161.2011.636081.

Zhao, L., Shi, Y., Liu, B., Hovis, C., Duan, Y., and Shi, Z. 2019. "Finer classification of crops by fusing UAV images and Sentinel-2A data." *Remote Sensing*, Vol. 11(No. 24): pp. 3012. doi:10.3390/rs11243012.

Zhang, L., Gong, Z.N., Wang, Q.W., Jin, D.D., and Wang, X. 2019. "Wetland mapping of Yellow River Delta wetlands based on multi-feature optimization of Sentinel-2 images." *Journal of Remote Sensing*, Vol. 23: pp. 313–326.